

A closed-form, analytical approximation for apparent surface charge and electric field of molecules.

Dan Folescu¹ and Alexey V. Onufriev^{1, 2, 3, a)}

¹⁾*Department of Computer Science, Virginia Tech*

²⁾*Department of Physics, Virginia Tech*

³⁾*Center for Soft Matter and Biological Physics, Virginia Tech, Blacksburg, VA 24061, USA*

Closed-form, analytical approximations for electrostatic properties of molecules are of unique value, as these can provide computational speed, versatility, and physical insight. Here we derive a simple, closed-form formula for the apparent surface charge (ASC), as well as for the electric field generated by a molecular charge distribution in aqueous solution. The approximation, with no fitted parameters, is tested against corresponding numerical solutions of the Poisson equation, where it yields a significant speed-up. For small molecules, the hydration free energies estimated from the closed-form ASC formula are within 0.6 kcal/mol RMSD from the standard Poisson reference; the electric field at the surface is in quantitative agreement with the reference. Performance of the approximation is also tested on larger structures, including a protein, a DNA fragment, and a protein-protein complex. For all structures tested, a near quantitative agreement with the numerical Poisson reference is achieved, except in regions of high negative curvature, where the new approximation is still qualitatively correct. A unique feature of the proposed "source-based" closed-form approximation, is that the ASC and the electric field are estimated at any individual point or surface patch, without the need for self-consistent computation over the entire surface or volume. An open source software implementation of the method has been made available: <http://people.cs.vt.edu/~onufriev/CODES/aasc.tar.gz>.

^{a)}Electronic mail: alexey@vt.cs.edu

I. INTRODUCTION

Accurate and efficient modeling of solvation effects at the atomistic level is a critical component of modern efforts to understand biomolecular structure and function¹⁻⁴. There are two broad approaches to the modeling of solvation: explicit and implicit solvation methods⁵. Arguably the most widely used model of solvation is that for which individual solvent molecules are treated explicitly, on the same footing with the target biomolecule. However, accuracy of the explicit solvent representation comes at high price, computationally, limiting the practical utility of atomistic simulations in many areas. The implicit, continuum solvation approach – treating solvent as a continuum with the dielectric and non-polar properties of water – can offer much greater effective simulation speeds compared to the explicit solvent models⁶⁻¹⁶. The Poisson equation^{7,8,17-21} of classical electrostatics²² provides an exact formalism – within the continuum, local, linear-response dielectric approximation of solvent in the absence of mobile ions – for computing the electrostatic potential $V(\mathbf{r})$ produced by a molecular charge distribution $\rho(\mathbf{r})$ characterizing the solute:

$$\nabla\epsilon(\mathbf{r})\nabla V(\mathbf{r}) = -4\pi\rho(\mathbf{r}), \quad (1)$$

where $\epsilon(\mathbf{r})$ is the dielectric constant. Once $V(\mathbf{r})$ is obtained, the electrostatic part of the solvation free energy is easily computed²². For the given charge distribution, $\rho(\mathbf{r})$, fundamental to a given biomolecule, there is induced a corresponding *electric reaction field*.

The problem of finding $V(\mathbf{r})$ is mathematically equivalent^{23,24} to finding a continuous charge density, σ , on the dielectric boundary (DB), such that:

$$V(\mathbf{r}) = \sum_i \frac{q_i}{|\mathbf{r} - \mathbf{r}_i|} + \oint_{\partial S} \frac{\sigma(\mathbf{s})}{|\mathbf{r} - \mathbf{s}|} d^2s, \quad (2)$$

where $\rho(\mathbf{r})$ is the discrete charge distribution, formed by n point charges q_1, \dots, q_n , and $\sigma(\mathbf{s})$ is the *apparent surface charge* (ASC) associated with each surface patch \mathbf{s} . The second term in the above equation represents the so-called reaction field potential^{25,26}. Conceptually, once the ASC, $\sigma(\mathbf{s})$, is found, all of the solvation effects, at the level of the Poisson equation, can be computed. This dielectric polarizable continuum method (DPCM) is now considered part of the broader apparent surface charge (ASC) formalism²⁷.

The reformulation of the Poisson problem via equation 2 has a number of technical advantages made apparent over the years, especially in quantum mechanical (QM) calculations.

For example, non-equilibrated behavior can be modeled through self-consistency calculations via the DPCM²³. Approximate descriptions of volume polarization, resulting from solute charge penetration²⁸, can be expressed within the integral equation formalism (IEF)²⁹ and “surface and simulation of volume polarization for electrostatics” (SS(V)PE)³⁰ methods. In practice, these advantages have led to many fruitful applications in the elucidation of solvation mechanisms^{6,31–36}, and the construction of tailored electrostatic models^{37,38}.

Just like the numerical Poisson solvers, modern ASC-based methods rely on increasingly realistic, yet complex, molecular boundary representations^{39–41}. These physically accurate representations of the actual molecular shape are crucial to the accuracy of modern solvation models, and have made significant impacts in qualitative reasoning about biomolecules^{42,43}. Unfortunately, rigorous ASC-based numerical approaches tend to be rather expensive, computationally^{23,24,44}, and may suffer from instabilities associated with the surface representations^{27,29,45}. The computational cost and associated stability concerns of many popular numerical ASC-based models^{27,46,47} is one of the major motivations for this work.

To improve computational efficiency, approximate ASC-based methods have been developed, such as the widely used COSMO⁴⁸, GCOSMO³⁶, and C-PCM⁴⁹. These methods rely on approximations to equation 2, such as the use of infinite dielectric ($\epsilon \rightarrow \infty$). These approaches bypass the difficult-to-calculate solute electric field normals⁵⁰, improving computational efficiency significantly. Still, these methods depend on numerical matrix inversions, which tend to scale poorly with the structure size^{51,52}.

At the same time, fully analytical approximations to the Poisson equation exist, the generalized Born model^{53–81} being arguably the most widely used, especially in atomistic simulations^{82–92}. Despite its multiple documented success stories⁹³ the model does not have the versatility of equation 2, and the associated benefits of an ASC-based formulation of biomolecular electrostatics. We aim to fill the gap by deriving an *analytical*, closed form approximation to the Poisson equation for the ASC and the (normal) electric field around an arbitrary biomolecule. Standard numerical solutions of the Poisson equation are used as the reference. We refrain from comparisons with well-established numerical ASC methods in this initial investigation.

The outline of the paper is as follows. Section II describes testing materials and methodology. In section III, we derive our analytical ASC approximation (III A), and test against

analytical (III B 1) and numerical (III C 2 a, III C 2 b) references. Finally, section III D showcases our analytical ASC approximation on a presently relevant biomolecular complex: that of the human ACE2 receptor and SARS-CoV-2 spike glycoprotein.

II. METHODS

A. Structures

We utilize a set of 173 neutral small molecules from version 0.52 of the FreeSolv database^{94,95}, narrowed to include only those molecules containing hydrogen, oxygen, nitrogen, and carbon atoms. The small molecules under consideration are all rigid - having small conformational variability as seen in molecular dynamic (MD) simulations⁹⁶. The choice of rigid molecules allows us to focus on the physics of solvation, while mitigating the uncertainty related to conformational sampling. *ambpdb*⁹⁷ was used to generate PQR format files from AMBER format coordinate and topology files⁹⁴. Additionally, two larger biomolecules were used: a 25 bp poly-A B'-form dsDNA⁴³; and the hen-egg lysozyme (PDB:2LZT)⁹⁸. We also test our method on a portion of the ACE2/SARS-CoV-2 complex (PDB:6M0J)⁹⁹ receptor binding domain (RBD). 6M0J RBD residues were determined through A/E chain contacts within 3.8 Å. In each chain, residues within 1.5 Å of the contacts were also included. H++ server¹⁰⁰ was used to generate protonated PQR format files. PQR format files for small molecules and the SARS-CoV-2 complex, along with RBD contact residue lists, are provided in the code supplement.

B. Dielectric Boundary Representations

We approximate the solute-solvent interface – the dielectric boundary (DB) – using the solvent excluded surface (SES)¹⁰¹, with Bondi¹⁰² atomic radii and a water probe of 1.4 Å. This DB is triangulated with the open-source package, NanoShaper¹⁰³. In each relevant test, we match the NanoShaper grid spacing with that used by the numerical PB reference; 0.1 Å for small molecules, 0.25 Å for fair speed comparisons, and 0.5 Å for large molecule electric field normal comparisons.

C. Analytical Poisson-Boltzmann Reference

In the context of implicit biomolecular solvation, the simplest scenario is that of a biomolecule with a sharp, spherical DB.

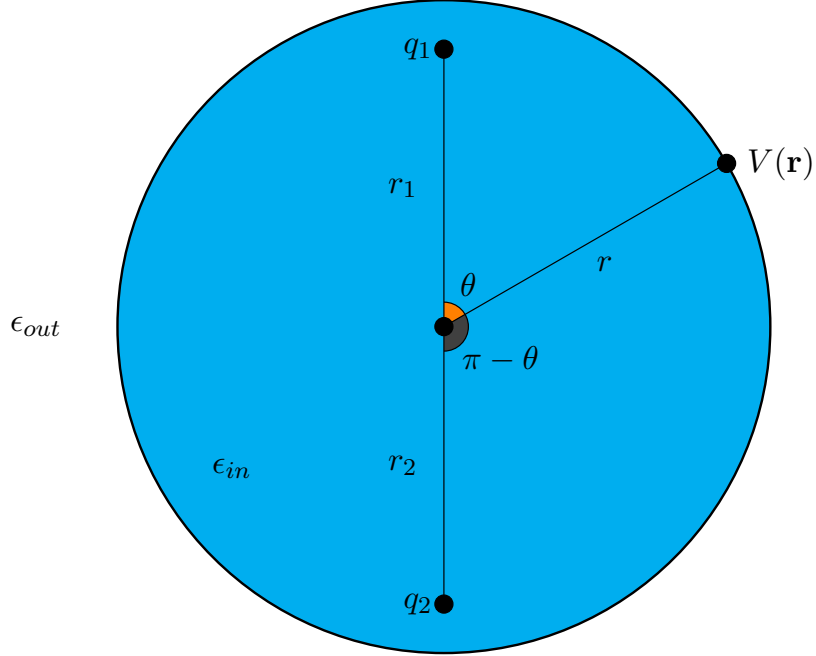


Figure 1: A perfectly spherical DB enclosing two unit charges, q_1 and q_2 . The charges are located on the vertical diameter of the sphere of radius r . The charges are an equal distance, $r_1 = r_2$, from the spherical center. The sharp spherical boundary, ∂S , separates two regions of constant dielectric, ϵ_{in} and ϵ_{out} . The “dual positive” test case: $q_1 = q_2 = 1$. The “dipole” test case: $q_1 = 1$ and $q_2 = -1$. The electric potential $V(\mathbf{r})$ is computed at the DB.

For such a spherical boundary, as in Figure 1, Kirkwood¹⁰⁴ gave the exact, analytical solution of equation 1 for the potential V_i at the DB due to a single charge q_i inside the boundary. We state it here without the consideration of mobile ions, not considered in this work¹⁰⁵:

$$V_i = -\frac{q_i}{r} \left(\frac{1}{\epsilon_{in}} - \frac{1}{\epsilon_{out}} \right) \sum_{l=0}^{\infty} \left[\frac{1}{1 + \left(\frac{l}{l+1} \right) \left(\frac{\epsilon_{in}}{\epsilon_{out}} \right)} \right] \left(\frac{r_i}{r} \right)^l P_l(\cos \theta) + \frac{q_i}{r} \left(\frac{1}{\epsilon_{in}} \right) \sum_{l=0}^{\infty} \left(\frac{r_i}{r} \right)^l P_l(\cos \theta). \quad (3)$$

For general internal and external dielectrics, it is well-known^{22,23} that the apparent surface

charge, σ , can be written as:

$$\sigma = \frac{1}{4\pi} \left(\frac{\epsilon_{out}}{\epsilon_{in}} - 1 \right) \left(\frac{\partial V}{\partial \vec{n}} \right)_{out}. \quad (4)$$

From this, and equation 3, we obtain an *exact*, analytical expression for the apparent surface charge on the spherical DB:

$$\sigma_{KW} = \sum_i \frac{q_i}{4\pi} \left(\frac{1}{\epsilon_{in}} - \frac{1}{\epsilon_{out}} \right) \left[\sum_{l=0}^{\infty} \left[\frac{1}{1 + \left(\frac{l}{l+1} \right) \left(\frac{\epsilon_{in}}{\epsilon_{out}} \right)} \right] (l+1) \left(\frac{r_i^l}{r^{l+2}} \right) P_l(\cos \theta) \right. \\ \left. - \left(\frac{1}{\epsilon_{in}} \right) \sum_{l=0}^{\infty} (l+1) \left(\frac{r_i^l}{r^{l+2}} \right) P_l(\cos \theta) \right], \quad (5)$$

where the summation is over all of the enclosed charges. Equation 5 will provide a key check for our analytical ASC approximation.

1. *Convergence Analysis of σ_{KW}*

The presence of the indexing term, $(l+1)$, is notable in its effects on the convergence characteristics of equation 5, by increasing the number of terms necessary for an accurate reference. As the ratio r_i/r approaches 1 - that is, as the charge approaches the DB - slow convergence of the approximate solution manifests itself.

Convergence of the analytical Poisson-Boltzmann reference for apparent surface charge

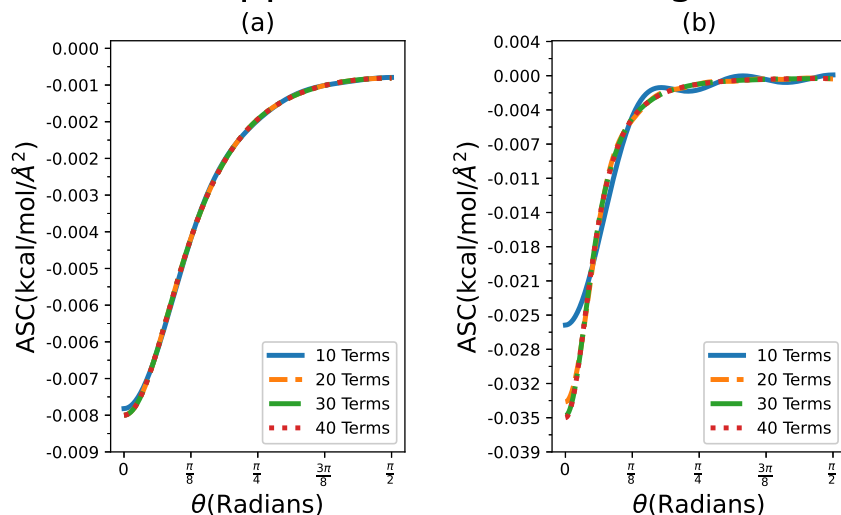


Figure 2: The apparent surface charge computed using the truncated analytical Poisson-Boltzmann reference (see equation 5). Tests are conducted on the dual-positive case, Figure 1. The ASC is sampled at the spherical boundary $r = 10 \text{ \AA}$ away from the center. Panel (a) $r_1 = r_2 = 6 \text{ \AA}$; (b) $r_1 = r_2 = 8 \text{ \AA}$; see Figure 1. Partial sums of the infinite series solution, equation 5, with $M = 10, 20, 30, 40$ terms are examined. The truncated sums are shown with blue, orange, green, and red lines, respectively.

In Panel (b) of Figure 2, we see that, even for $\frac{r_i}{r}$ close to 1, it is possible to achieve both qualitatively and quantitatively reasonable results. The analytical reference appears well-converged, Figure 2, for our purposes, at $M = 30$ terms. We term equation 5, truncated to the first $M = 30$ terms, as the essentially exact Poisson-Boltzmann (EPB) reference.

D. Numerical Poisson-Boltzmann Reference

For numerical Poisson-Boltzmann (NPB) reference calculations, we use the Macroscopic Electrostatics with Atomic Detail (MEAD) package¹⁰⁶. MEAD is a volumetric, finite-difference solver that can compute potential maps and hydration energies. For small molecule accuracy comparisons, we perform potential-map calculations at a grid spacing of 0.1 \AA , and hydration energy calculations at an inner and outer bounding-box grid spacing of 0.1 \AA and

0.5 Å, respectively. For fair speed comparisons, we perform potential-map calculations at a grid spacing of 0.25 Å, and hydration energy calculations at a single bounding-box grid spacing of 0.25 Å, considered standard for finite-difference NPB calculations. For larger molecules, we perform potential-map calculations at a grid spacing of 0.5 Å, and hydration energy calculations at an inner and outer bounding-box grid spacing of 0.5 Å and 1.0 Å, respectively. The total number of NPB grid points was determined by setting a volumetric bounding-box side length slightly larger (+1 Å) than the maximal intra-molecular distance. We have approximated the electric field normal at a point, \mathbf{r} , by :

$$\mathbf{E}_{\perp}(\mathbf{r}) = \frac{\partial V}{\partial \vec{n}} \approx \frac{V(\mathbf{r} + h\hat{n}) - V(\mathbf{r} - h\hat{n})}{2h}, \quad (6)$$

where $\mathbf{r} + h\hat{n}$ and $\mathbf{r} - h\hat{n}$ are sampling points a distance $2h$ from one another, in the normal direction. See Ref.⁵² for the sampling details. Here h was chosen to minimize the distance between sampled grid points, while being large enough so that the sampled points belong to distinct grid points of the cubic lattice used in NPB reference calculations. For small molecules, with a grid spacing of 0.1 Å, in the worst-case, h must be larger than the diagonal of the “grid cube”: $\sqrt{3}/(0.1)^2 \sim 0.173$ Å. To avoid numerical artifacts, the field is computed a distance $p > h$ from the DB, Figure 3. The need to use a non-zero *projection distance* in the NPB calculations makes it necessary to use the electric field normal values near the DB as the numerical reference, rather than the apparent surface charge itself (which is essentially the normal component of the field right at the DB, see equation 4).

E. Electrostatic Solvation Free Energy with ASC

The apparent surface charge formulation allows us to gain electrostatic insights into a variety of solvation effects^{25,47}, one of which is *hydration free energy*. This quantity can be expressed through the thermodynamic cycle decomposition¹⁰⁷:

$$\Delta G_{solv} = \Delta G_{el} + \Delta G_{np}. \quad (7)$$

Of the two components in equation 7, the *electrostatic solvation free energy*, ΔG_{el} , typically contributes the most to the total, and is difficult to estimate computationally⁵.

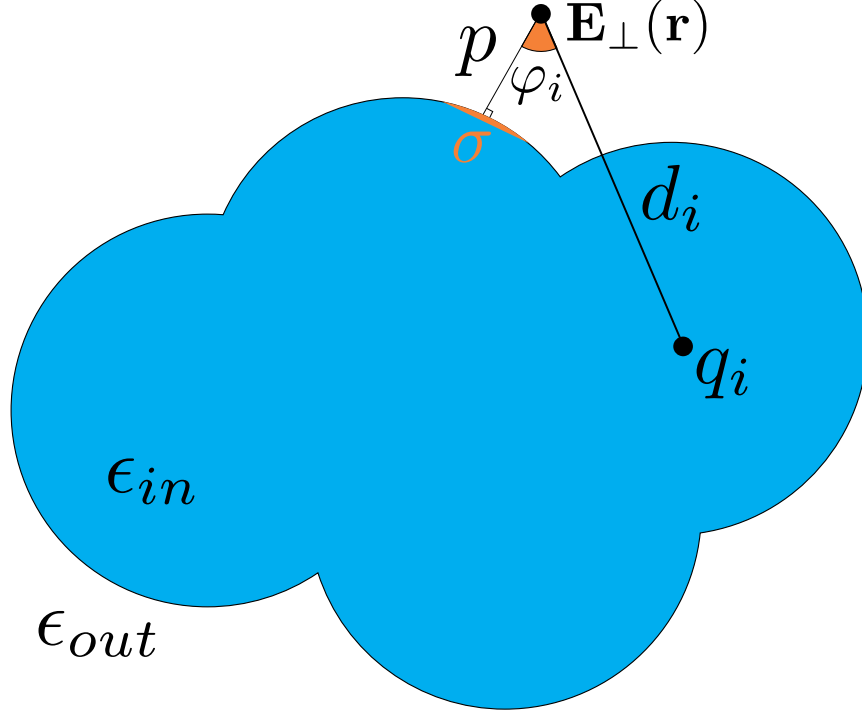


Figure 3: The two dielectric problem, given an arbitrary biomolecule S with smooth boundary ∂S . The boundary separates inner (blue) and outer (white) dielectric regions, with constants ϵ_{in} and ϵ_{out} , respectively. $r = A + p$, where A is the *electrostatic size* of S ¹⁰⁸, and p is the *projection distance* from ∂S to the sampling point, \mathbf{r} . q_i is the source charge under consideration, with \mathbf{r}_i (not shown) denoting its position, and d_i denoting the distance between \mathbf{r}_i and \mathbf{r} . When $p > 0$, we call the quantity $E_{\perp}(\mathbf{r})$ the *electric field normal* of S at \mathbf{r} . When $p = 0$, we relate electric field normals using equation 4; in this case, $\sigma(\mathbf{r})$ (not shown) is termed the *apparent surface charge* of S at \mathbf{r} .

For a discrete charge density indexed by i , see Figure 3, we can define ΔG_{el} as⁵:

$$\Delta G_{el} = \frac{1}{2} \sum_i q_i [V(\mathbf{r}_i) - V(\mathbf{r}_i)_{vac}], \quad (8)$$

where $V(\mathbf{r}_i)$ and $V(\mathbf{r}_i)_{vac}$ are electrostatic potentials in solvent and vacuum, respectively. In the special case when inner and outer dielectric constants, ϵ_{in} and ϵ_{out} , are equal to 1 and 80, respectively, we call ΔG_{el} the *electrostatic hydration free energy*. We use equations 2 and 8 to write:

$$\Delta G_{el} = \frac{1}{2} \sum_i q_i \left(\oint_{\partial S} \frac{\sigma(\mathbf{s})}{|\mathbf{r}_i - \mathbf{s}|} d^2s \right). \quad (9)$$

Though equation 9 is valid for any choice of DB, the surface integral is non-trivial to compute. We approximate the surface integral using a specific triangulation of the DB, see section II B. This discrete representation approximates equation 9 as:

$$\Delta G_{el} \approx 332 \left[\frac{1}{2} \sum_i \sum_T \frac{q_i \sigma_T A_T}{|\mathbf{r}_i - \mathbf{r}_T|} \right], \quad (10)$$

where σ_T , A_T , and \mathbf{r}_T are the apparent surface charge, area, and center of the triangle T ; for convenience, the pre-factor converts the sum to kcal/mol, if the units of length are Å, and the charge is in atomic units. ASC on a triangle is found by averaging the ASC of comprising vertices. The center is a simple geometric average of comprising vertex coordinates, with triangular area calculated using Heron’s formula:

$$A = \sqrt{d \cdot (d - a) \cdot (d - b) \cdot (d - c)} \quad ; \quad d = \frac{a \cdot b \cdot c}{2}, \quad (11)$$

where a , b , and c are the triangle’s side lengths.

F. Generalized-Born Solvation Free Energy Reference

We utilize the IGB5¹⁰⁹ GB model from AMBER package⁹⁷. Configuration files for the GB reference are included in the supplement.

G. Accuracy Metrics Used

We test our ASC approximation, first against the EPB reference, and then against NPB and GB references. Our comparison with the EPB reference will be on point-wise apparent surface charge, using the two charge configuration in Figure 2. Per-vertex electric field normal values are compared against the NPB reference, averaging over each vertex in a given biomolecule, and over each biomolecule in the comparison set. Electrostatic hydration free energies are compared against the NPB and GB references, taking averages over molecule sets. All results will be in kcal/(mol $\cdot e \cdot \text{Å}^2$) for apparent surface charge, kcal/(mol $\cdot e \cdot \text{Å}$) for electric field normals, and kcal/mol for electrostatic hydration free energies.

H. Computer Specifications

All computations and visualizations were completed on a commodity desktop computer with an Intel Core i7 (or equivalent) processor, using a maximum of 32 GB of memory.

III. RESULTS

A. Analytical Derivation of Apparent Surface Charge

To derive our ASC approximation, we begin with the closed-form approximation for the electrostatic potential around an arbitrary molecular shape¹⁰⁵, see Figure 3:

$$V_i \approx \left(\frac{q_i}{\epsilon_{out} \left(1 + \alpha \left(\frac{\epsilon_{in}}{\epsilon_{out}} \right) \right)} \right) \left[\frac{(1 + \alpha)}{d_i} - \frac{\alpha \left(1 - \frac{\epsilon_{in}}{\epsilon_{out}} \right)}{r} \right]. \quad (12)$$

We utilize the polar orthonormal frame, $e_r = \frac{\partial}{\partial r}$; $e_\theta = \frac{1}{r} \frac{\partial}{\partial \theta}$, to take its derivative, for use in equation 4. The derivative vanishes in the direction of e_θ , yielding:

$$\mathbf{E}_\perp(\mathbf{r}) = \frac{\partial V_i}{\partial \vec{n}} = \frac{\partial V_i}{\partial r} - \cos(\varphi_i) \frac{\partial V_i}{\partial d_i}. \quad (13)$$

Exploiting the geometry in Figure 3, we relate $\cos(\varphi_i)$ as a dot product of the surface unit normal, \hat{n} , and the vector from $\mathbf{E}_\perp(\mathbf{r})$ to q_i , which we denote \vec{d}_i : $\cos(\varphi_i) = (\hat{n} \cdot \vec{d}_i) / d_i$. Applying equation 12 to 13, and summing over the charge distribution (Figure 3) we arrive at:

$$\mathbf{E}_\perp(\vec{r}) = \left(\frac{1}{\epsilon_{out} \left(1 + \alpha \left(\frac{\epsilon_{in}}{\epsilon_{out}} \right) \right)} \right) \sum_i q_i \left[\left(\frac{\alpha \left(1 - \frac{\epsilon_{in}}{\epsilon_{out}} \right)}{r^2} \right) - \cos(\varphi_i) \left(\frac{(1 + \alpha)}{d_i^2} \right) \right]. \quad (14)$$

At the dielectric boundary, applying equation 4 to equation 14, gives the following closed-form, analytical approximation for the apparent surface charge:

$$\sigma = \left(\frac{1}{\epsilon_{in}} - \frac{1}{\epsilon_{out}} \right) \left(\frac{1}{4\pi \left(1 + \alpha \left(\frac{\epsilon_{in}}{\epsilon_{out}} \right) \right)} \right) \sum_i q_i \left[\left(\frac{\alpha \left(1 - \frac{\epsilon_{in}}{\epsilon_{out}} \right)}{A^2} \right) - \cos(\varphi_i) \left(\frac{(1 + \alpha)}{d_i^2} \right) \right]. \quad (15)$$

We have attempted to re-optimize the value of α in the context of equation 15 using our small molecule set: the effort led to only a very minor improvement in accuracy (not shown), so we have decided to retain the original, rigorously derived¹¹⁰ $\alpha = 0.580127$, for use in the approximation.

B. Theoretical Analysis of the Analytical ASC Approximation

1. Accuracy against the exact PB Reference

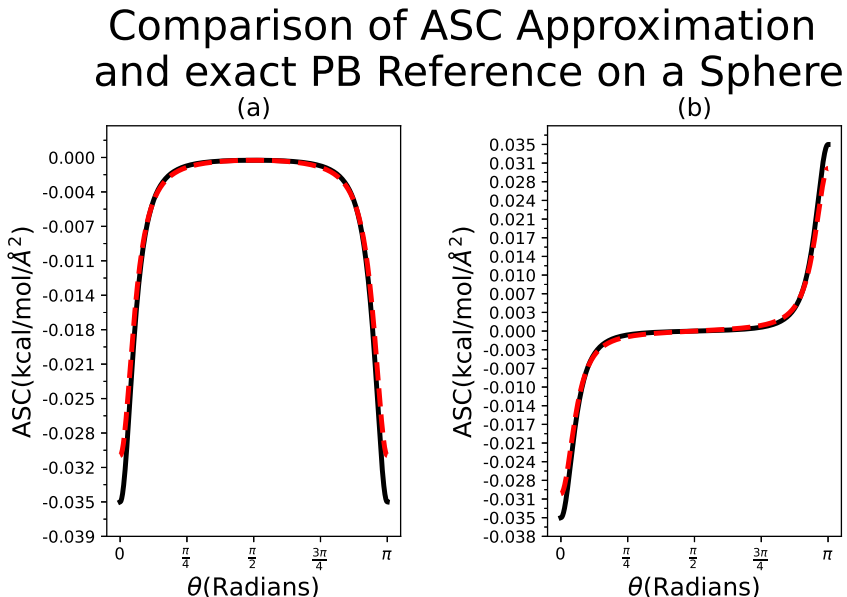


Figure 4: Apparent surface charge of our ASC approximation (dashed red) and the EPB reference (solid black) on the test charge distribution shown in Figure 1. Panel (a): surface charge of two point charges, 2 \AA away from the boundary of a sphere with $q_1 = 1 = q_2$. Panel (b): the same charge distribution as in panel (a), but with $q_1 = 1, q_2 = -1$. Points were sampled from 0 to π in 0.0001 radian steps.

From Figure 4, our approximation matches the exact solution quite well over the interval of interest, with the expected slightly worse performance near point charges. Over the entire interval, an RMSD of 0.00124 and 0.00117 kcal/mol/ \AA^2 was achieved between our ASC approximation and the EPB reference, on the geometries described in panels (a) and (b), respectively (Figure 4).

2. Total Molecular Charge Sanity Check

Gauss' law provides an excellent check of our analytical ASC approximation and utilized dielectric boundary representation, for arbitrary biomolecules. If we consider $\epsilon_{in} = 1$ with $\epsilon_{out} \rightarrow \infty$, Gauss' law, for a discrete internal charge distribution (see Figure 3), gives:

$$\oint_{\partial S} \mathbf{E}_{\perp}(\mathbf{s}) \cdot d^2\mathbf{s} = \sum_i q_i + \oint_{\partial S} \sigma d^2s = 0. \quad (16)$$

Over our set of neutral molecules, equation 16 simply states that the surface integral of apparent surface charge will be equal to zero; in the discrete boundary case, as triangulation density is increased, we expect this quantity to approach zero.

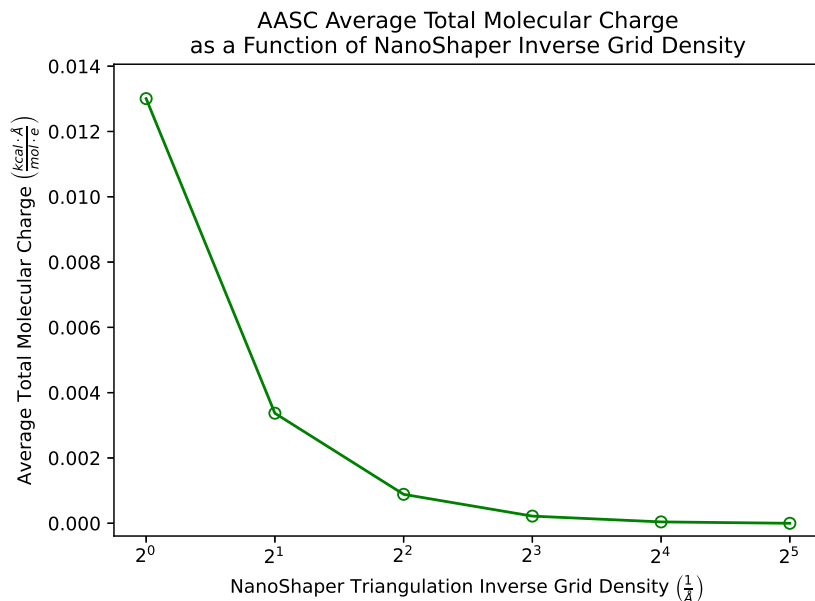


Figure 5: Total molecular surface charge averaged over the entire set of small neutral molecules. The exact result is zero. NanoShaper inverse grid spacings are given in Å^{-1} , while total molecular charges are given in $(\text{kcal} \cdot \text{Å}) / (\text{mol} \cdot e)$. To mimic a conductor, we set the outer dielectric constant $\epsilon_{out} = 1000$.

Figure 5 shows that our numerical ASC implementation follows the expected trend in conductor-like solvent.

C. Testing of AASC Package Implementation

1. Computational Speed

Here we present general running time descriptions for each tested method, rather than exact time values. In this way, we can differentiate between each method, without worrying about particular optimizations and expert parameter set-ups that can be found across a variety of implementations. The interested reader can refer to the supplement for the detailed timing information.

Method	Small Molecules	2LZT	DNA
IGB5(AMBER)	milliseconds	~ a second	~ half a second
Analytical ASC Approximation	~ 100 milliseconds	tens of seconds	~ half a minute
Numerical PB	tens of seconds	minutes	tens of minutes

Table I: Running time expectations for computed electrostatic solvation free energies. Times are given per-molecule (averaged over the entire set in the small molecule case).

In algorithmic time complexity, the three methods we compare in Table I are very different. GB methods, such as the IGB5 reference, scale quadratically in the number of atoms (K^2), while our method grows linearly (KN) in the number of atoms and surface elements (N). Volumetric methods, similar the NPB reference, scale cubically in the number of grid points per side of a corresponding bounding box, itself a function of grid density and the maximum intra-molecular distance. The impact of these time complexities are clearly seen when we focus on hen-egg lysozyme and double-stranded DNA wall running times. Though the 2LZT structure has about 500 more atoms than the DNA structure, the intra-molecular width of the DNA structure is almost double that of 2LZT. This means that the DNA structure has both a larger total surface area and requires a bigger volumetric bounding box; as seen in Table I, we find longer running times for our ASC approximation and the NPB reference for 2LZT as compared to DNA, but not for the IGB5 reference. This contrasting algorithmic complexity also affects timings between each model, for structures of different size. The best case scenario for the efficiency of our ASC approximation is for structures

having many atoms, but a comparatively low surface area.

Though the efficiency of our analytical ASC method is not at the level of the IGB5 reference, it occupies a different niche: its main purpose is the estimation of the ASC and the electric field. Compared to common ASC-based methods, such as those of a DPCM variety^{23,24,111}, our method features key advantages in theoretical efficiency. Self-consistent, iterative methods^{23,24} must iterate their solution for apparent surface charge. Work has been undertaken to improve the efficiency of such iterative algorithms^{111,112}, and address concerns of convergence^{113,114}; however, even when approximations are made¹¹¹ computational time grows quadratically (N^2) in the number of surface elements.

2. Accuracy

a. Small Molecules

Qualitative Visualizations We first examine how our ASC approximation compares to the NPB reference *qualitatively*.

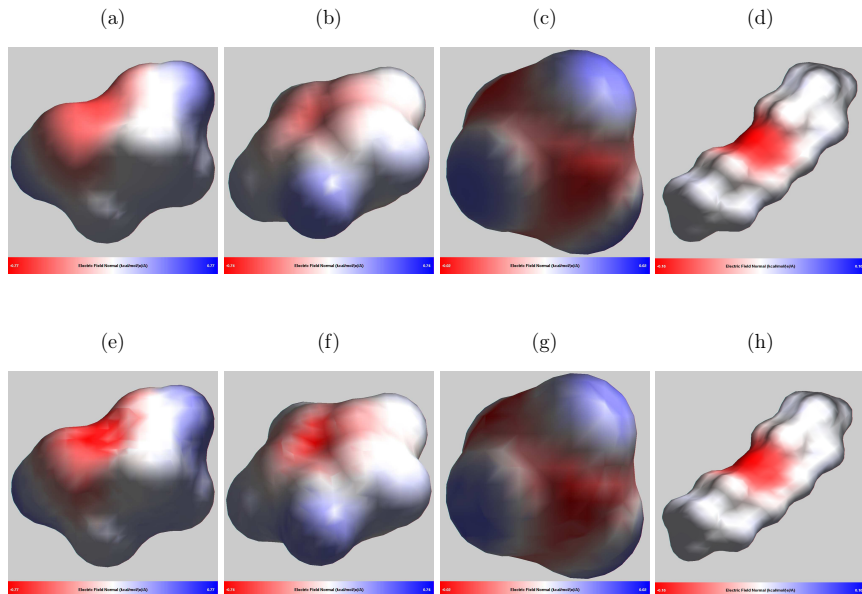


Figure 6: Electric field normals computed on a selection of small molecules by our ASC approximation (top row) and the NPB reference (bottom row), with visualization by GEM⁵². From left to right, the four molecules shown are 1,2-ethanediol, pyrrole, methane, and 1-Butoxybutane. All calculations are made 0.7 \AA from the DB, with a water probe radius of 1.4 \AA . Our ASC approximation and the NPB reference use a 0.1 \AA triangulation density/grid spacing.

Results from our ASC approximation are visually indistinguishable from those computed with the NPB reference. Numerical instabilities of the NPB manifest themselves as small discontinuities in the electric field normal values, most noticeable in the negatively charged surface patches, see panels (e) and (f) of Figure 6. Our method has no such instabilities due to the analytical formulation of our ASC approximation, and the robustness of its discrete boundary representation¹⁰³; One such example was readily seen through the very minimal absolute change in ASC small molecule solvation energies when the grid resolution was decreased from 0.1 \AA to 0.25 \AA .

Quantitative ASC Comparisons Next, we examine how our ASC approximation compares *quantitatively* to the NPB reference, Table II. While the field normal (or the equivalent surface charge) metrics are not very intuitive, these are the main quantities that

Metric	ASC Approximation relative to NPB Reference
Average Absolute Difference	0.11
Average RMSD	0.14

Table II: Accuracy of electric field normal values computed via our ASC approximation against the NPB reference. Values are given in kcal/(mol $\cdot e \cdot \text{\AA}^2$).

the method computes, and so a direct comparison with the standard NPB reference is useful. The physical meaning of the magnitude of the deviation from the reference will be discussed below. We note that some of the deviation is likely a result of the aforementioned NPB grid-related instabilities.

Polar Solvation Energy Tests featuring the calculation of electrostatic solvation free energies are valuable in the sense that they provide an intuitive accuracy metric, directly relevant to experiment. Here IGB5¹⁰⁹ is an example of what can be expected from a very fast GB model on small molecule data sets^{115,116}, in terms of accuracy and running time. We test how our ASC approximation and the IGB5 method compares to calculation of electrostatic solvation free energies by the NPB reference.

Method	RMSD to NPB reference (kcal/mol)
Analytical ASC Approximation	0.61
GB (IGB5,AMBER)	0.98

Table III: Accuracy of electrostatic hydration free energies against the NPB reference, estimated by our analytical ASC approximation and IGB5. Analytical ΔG_{el} is computed via equation 9, using the analytical ASC approximation given in equation 15. Small molecule electrostatic hydration free energies range from -0.01 to -14.71 kcal/mol.

In Table III, we see that our ASC approximation performs better than the IGB5 reference in the reproduction of NPB electrostatic solvation energy. This is encouraging, particularly from the perspective of design: GB models are formulated to analytically interpolate the

Poisson equation, for the purpose of electrostatic solvation energy calculations. That our model can estimate solvation energies more accurately than a widely used GB model suggests that the reproduction of electric field normals with the NPB reference is physically supported.

Additionally, the results of Table III give another encouraging conclusion, with respect to running times efficiencies. To match the RMSD of the NPB reference to just slightly above kT , we do not require an overly fine triangulation density. When resolution is taken as in timing section (I), RMSD against the NPB reference, in fact, improves to 0.6 kcal/mol. We can achieve a very similar accuracy, without incurring a heavy 1-2 order of magnitude time penalty, as seen with the NPB reference at this fine grid resolution.

b. Proteins and DNA In analyzing the performance of our model on structures of increased size and complexity, we examine a fragment of double-stranded DNA and the hen-egg lysozyme. Structures of this type - with regions of the DB having deep, negative curvature "pockets" - present some of the toughest tests for our model, due to certain theoretical considerations we touch on below.

Double-Stranded DNA First, we examine our analytical approximation on a double-stranded DNA snapshot.

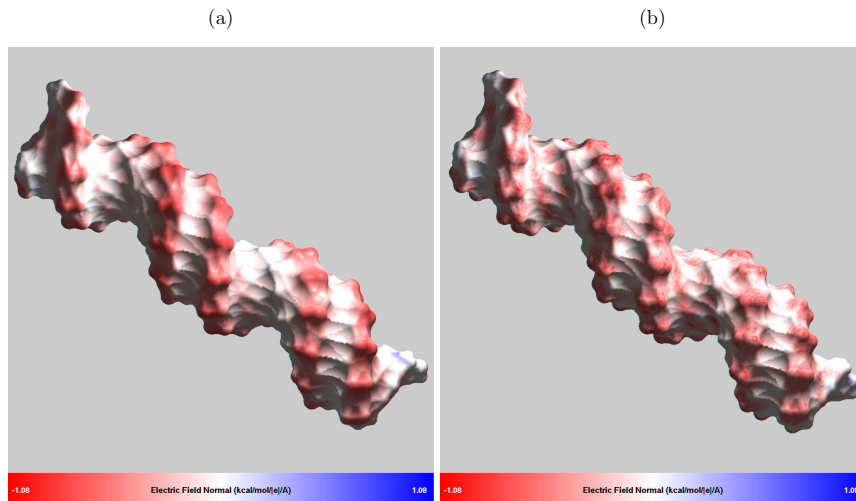


Figure 7: Electric field normals computed on the double-stranded DNA snapshot by our ASC approximation, Panel (a), and the NPB reference, Panel (b), with visualization by GEM⁵². The field is estimated 1.5 Å from the DB, obtained with the water probe of radius of 2 Å. Our ASC approximation and the NPB reference use a 0.5 Å triangulation density/grid spacing.

Qualitatively, Figure 7 shows that our analytical approximation reproduces the NPB reference quite well. Notably, there is a distinctive "striping" in the NPB reference, Figure 7b, as compared to our analytical ASC, which is smooth, Figure 7a. This spurious striping is likely a result of the projection of numerically derived potential maps upon the triangulated DB, seen prominently when compared to our small molecule tests (section III C 2 a) due to the increased grid spacing of these computations on larger structures.

Triclinic Hen Egg White Lysozyme Next, we make comparisons to the NPB reference on the triclinic hen egg white lysozyme.

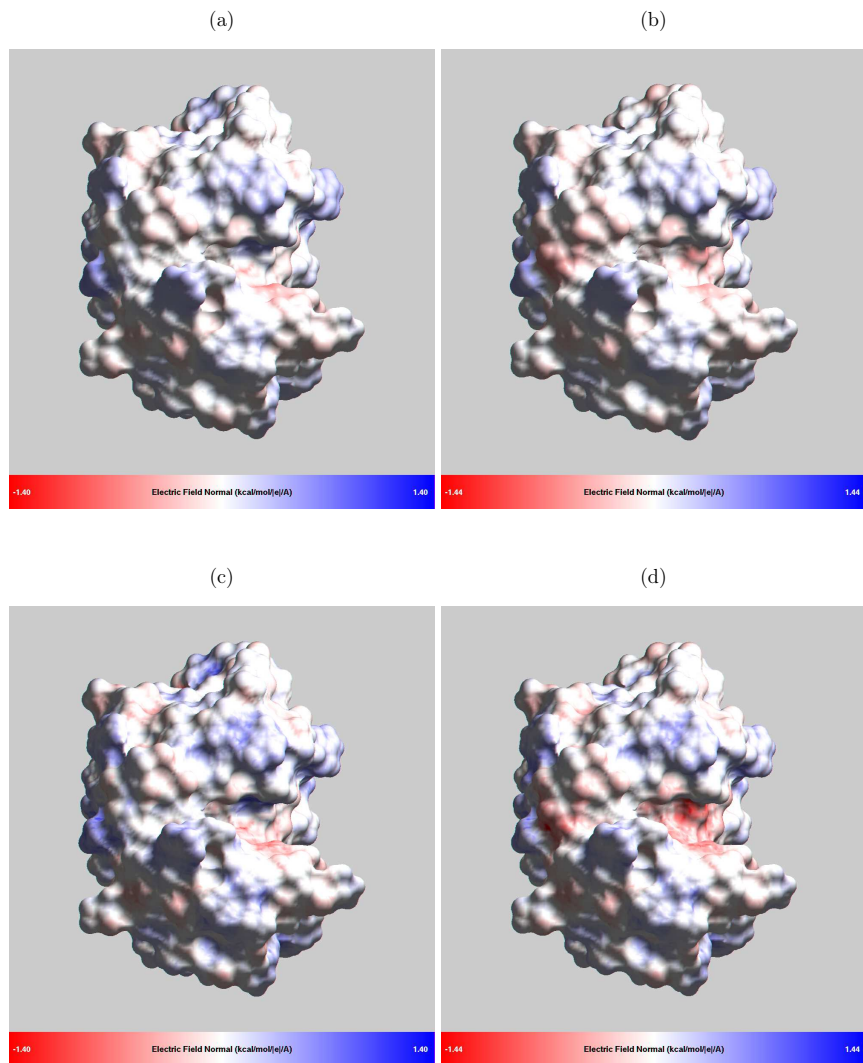


Figure 8: Electric field normals computed on the hen-egg lysozyme by our ASC approximation (top row) and the NPB reference (bottom row), with visualization by GEM⁵². Panels (a) and (c): the structure at pH 4.5. Panels (b) and (d): the structure at pH 6.5. All calculations are made 1.5 Å from the DB, with a water probe radius of 2 Å. Our ASC approximation and the NPB reference use a 0.5 Å triangulation density/grid spacing.

We see in Figure 8 that our analytical approximation accurately reproduces the NPB reference, outside of the hen-egg lysozyme’s binding cleft. Within the binding cleft, quantitative deviations in electric field normal magnitudes from the NPB reference become apparent, though our approximation still produces a qualitatively correct picture. From both our approximation (Figure 8a → 8b) and the reference (Figure 8c → 8d), the substantial

electrostatic effect of Asp 52 and Glu 35 in the enzymatic pocket can be visualized. Under mildly acid conditions (pH 4.5; Figures 8a and 8c), we see that Glu 35 changes electrostatically, as it donates a proton to form its conjugate base. This “inactive” binding cleft can be compared to its “active” counterpart, seen under slightly acidic conditions (pH 6.5; Figures 8b and 8d). The stability and behavior of Asp 52 and Glu 35, under pH change, is consistent with the Phillips mechanism^{117,118}.

Quantitative Comparisons With qualitative tests complete, we finish with a quantitative comparison between our analytical approximation and the NPB reference.

	Double-Stranded DNA	2LZT pH 4.5	2LZT pH 6.5
Absolute Difference	0.27	0.15	0.15
Average RMSD	0.37	0.19	0.20

Table IV: Electric field normal comparisons between our analytical approximation and the NPB reference, on double-stranded DNA and the protonated/un-protonated hen-egg lysozyme. All values are in kcal/(mol · e · Å).

As expected, quantitative performance deficiencies exist for larger molecules with prominent regions of negative curvature. Although the double-stranded DNA and hen-egg lysozyme have similar numbers of atoms, average RMSD values in Table IV are, relatively, inconsistent. On the double-stranded DNA snapshot (~ 1600 atoms), the average RMSD is about 2.6 times larger than on small molecules (Table II, IV). Comparatively, the hen-egg lysozyme’s average RMSD (~ 2000 atoms) is only about 1.4 times larger than on small molecules. On hydration free energies, absolute errors between our analytical approximation and the NPB reference are quite small on the DNA snapshot, $\sim 4\%$, but more than double, $\sim 12\%$, on the hen-egg lysozyme. These findings might have to do with the DNA’s proportion of negative curvature regions with respect to the whole.

To put the results of Tables II and IV in a better context, it may be helpful to consider a hypothetical situation. Suppose a biomolecule of interest has a constant electric field strength near its boundary. When compared to the reference, there is, on average, a maximum ~ 0.4 RMSD error in electric field normal values. If an electric charge was moved

1 Å away from the biomolecular boundary, along the surface normal, the total work would be bounded above by ~ 0.4 kcal / mol - small when compared to the “gold-standard” 1 kcal / mol difference against reference. In addition, we must also consider that the bound is *not* strict: electric field strength is inversely related to the square of distance from the surface, and would not stay constant as a charge is moved away.

Structural Considerations A notable feature, seen prominently in both the double-stranded DNA snapshot and the hen-egg lysozyme, but not generally in small molecules, is the presence of distinct negative curvature pockets on the DB. ASC calculations via our model are derived on a spherical DB (Figure 3), having positive curvature throughout. Negative curvature regions, such as the main groove in Figure 7 and the binding cleft in Figure 8, do not occur on a sphere; our model does not take into account regions of such characteristic. A resulting loss in performance had been noted previously⁵² for the approximate electrostatic potential (equation 12).

Confounding this effect, deep negative curvature regions on the DB can restrict water molecule conformational freedom, making nearby solvent behave less similar to that of the bulk^{119,120}. It has been shown that regions of this type can significantly modify interactions between small molecule inhibitors and their target proteins¹²¹, prompting investigations related to their identification^{122,123}. In our context, this change in the behavior of water bulk has negative implications on the performance of our model, but the same is true for the NPB reference, which is also based on the continuum solvent. Because both of these models are expected to deviate from the correct physical behavior within these regions of negative curvature, we argue that a qualitative agreement with the NPB reference may be acceptable here, in place of a strong quantitative agreement.

D. Testing on a large biomolecule

For a real-world application, we examine our approximation on a much larger (~ 6500 atom) complex, with important relevance today - the ACE2/SARS-CoV-2 complex (PDB ID:6M0J).

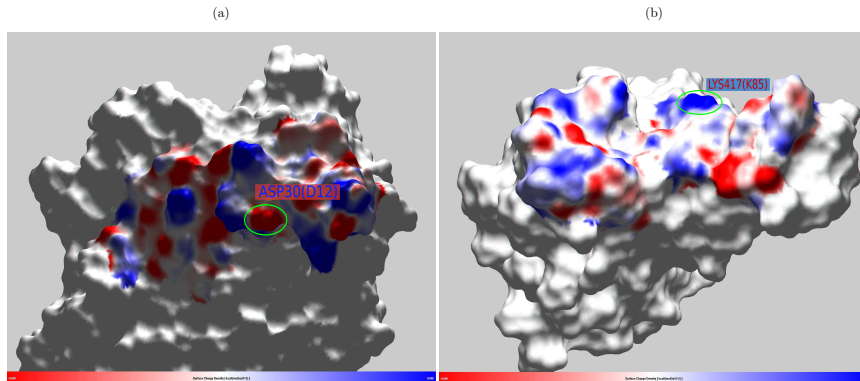


Figure 9: Apparent surface charge computed on the receptor binding domain (RBD) of ACE2 receptor/SARS-CoV-2 spike glycoprotein complex, with visualization by GEM⁵². Unlike formula 15, the sign is flipped to mimic Fig. 1 (B) of Wang et al⁹⁹. Figures 9a and 9b show the ACE2 receptor and SARS-CoV-2 spike glycoprotein RBDs, respectively. All calculations are made 0.7 Å from the DB with a water probe radius of 2 Å. A NanoShaper triangulation density of 0.5 Å is used.

Recently, a comparison has been made between SARS-CoV and SARS-CoV-2, examining various mutations and their effects on respective binding strengths with the ACE2 agonist⁹⁹. The focus of Figure 9 is on, what Wang⁹⁹ terms, the “CR2” receptor binding domain, and shows how our approximation reproduces the electrostatic complementary of surfaces charges between two residues, ASP30 (D12), Figure 9a, and LYS 417 (K85), Figure 9b, thought to contribute to the formation of a salt bridge. This salt bridge improves both stability and binding strength between the ACE2 receptor and SARS-CoV-2 spike protein, when compared to the SARS-CoV spike protein.

These large-scale visualizations of the ASC (or of the normal component of the electric field) has already been shown useful¹²⁴; our approximation might be a useful tool in understanding complex protein-protein interactions at a atomistic scale, including SARS-CoV-2 mutants of concern¹²⁵. Our method can contribute in this area due to its targeted, *source-based* approach in apparent surface charge computation. Compared to the reference NPB solver and ASC methods that rely on iterations for self-consistency, computation of apparent surface charges depend *only* on the underlying charge distribution. Independent electrostatic computation becomes possible, as Figure 9 shows, reducing computational time

drastically.

IV. CONCLUSION

In this work, we have derived a closed-form, *analytical* approximation for biomolecular apparent surface charge (ASC), and the normal component of the electric field. To the best of our knowledge, this is the first such fully analytical approximation. The approximation closely reproduces the infinite series solution for a perfect spherical boundary. Quantitative agreement with the standard numerical PB reference is achieved on most of the tested biomolecules, except within prominent regions of negative curvature, where the new approximation is still qualitatively correct. Comparisons with a popular fast GB model in AMBER (IGB5) shows that that our method is more accurate in reproducing the hydration free energy, albeit at higher computational expense. At the same time, standard numerical PB is still 1-2 orders of magnitude slower than the proposed approximation, which puts it "in-between" fast analytical GB and numerical PB. We stress that solvation free energy estimates are used here as a common and convenient accuracy metric, and is not where we believe the potential benefits of the analytical ASC may be. These benefits stem from the unique features of the method.

There are at least two features of the new approximation absent from the GB: the ability to estimate the apparent surface charge (and, hence, the potential everywhere); and the ability to estimate the normal component of the electric field. One unique feature of the approach sets it apart from other existing approximations that can estimate ASC, including those aimed at computing ASC directly – the fact that the new approximation is "source-based". This means that the normal electric field and the ASC can be estimated at any individual point or surface patch, without the need for self-consistent computation over the entire surface or volume. This feature is in contrast to "field-based" methods such as numerical solutions of the Poisson equation or DPCM. As an illustration, we showed that the "source-based" feature of our ASC approximation allows a rapid examination of the ACE2/SARS-CoV-2 RBD electrostatics, reproducing conditions posited to contribute to the spike protein's high binding strength. Another area which can, in our view, benefit from the proposed analytical ASC is the development of new implicit solvation methods that require fast estimates of local polarization charges or/and fields.

As it stands, the proposed method has several limitations. First, it does not yet include salt effects explicitly. However, in the future, it should be relatively easy to add into the model salt dependence at the Debye-Huckel level, following an approach outlined in Ref.¹⁰⁵. Another limitation of the model is its qualitative nature in the regions of high negative curvature, at least relative to the standard NPB reference. Overcoming this specific limitation will require a significant extension of the underlying theory. Additionally, while not specifically a limitation of a proof-of-concept work, a head-to-head comparison with existing methods for computing ASC is yet to be performed.

This initial exploration into the applications of electrostatic approximations within the apparent surface charge formalism gives a glimpse of what such a combination might achieve. Thus far, we see that the approximation can offer several potential advantages in computational efficiency over traditional numerical Poisson solvers, while proving more accurate and comprehensive than other analytically motivated counterparts. A careful and detailed comparison within the broader category of ASC methods is warranted; but, nonetheless, promising results have pointed to the potential of our approach in forming the basis of novel implicit models of solvation. We hope that this paper, along with the included code implementation will encourage further investigation into analytically motivated apparent surface charge approximations, and their applications.

V. ACKNOWLEDGMENTS

We would like to thank Nitin Passa for his contributions to the numerical ideas behind this application of ASC. In addition, we appreciate the help of Dr. Igor Tolokh for supplying the double-stranded DNA snapshot, and Dr. Andrew Fenley for his useful comments and suggestions. This work was supported by NIH Grant R21GM131228.

VI. DATA AVAILABILITY

The data that support the findings of this study are available from the corresponding author upon reasonable request.

REFERENCES

- ¹S. A. Adcock and J. A. McCammon, *Chem Rev* **106**, 1589 (2006).
- ²M. Karplus and J. A. McCammon, *Nat Struct Biol* **9**, 646 (2002).
- ³E. P. Raman and A. D. MacKerell, *J Am Chem Soc* **137**, 2608 (2015).
- ⁴R. E. Amaro and A. J. Mulholland, *J. Chem. Inf. Model.* **60**, 2653 (2020).
- ⁵A. V. Onufriev and S. Izadi, *Wiley Interdisciplinary Reviews: Computational Molecular Science* **8**, e1347 (2017).
- ⁶C. J. Cramer and D. G. Truhlar, *Chem. Rev.* **99**, 2161 (1999).
- ⁷B. Honig and A. Nicholls, *Science* **268**, 1144 (1995).
- ⁸P. Beroza and D. A. Case, *Methods Enzymol* **295**, 170 (1998).
- ⁹J. D. Madura et al., *Biological Applications of Electrostatic Calculations and Brownian Dynamics Simulations*, in Reviews in Computational Chemistry, pages 229–267, John Wiley & Sons, Ltd, 1994.
- ¹⁰M. K. Gilson, *Curr Opin Struct Biol* **5**, 216 (1995).
- ¹¹M. Scarsi, J. Apostolakis, and A. Caffisch, *J. Phys. Chem. A* **101**, 8098 (1997).
- ¹²R. Luo, L. David, and M. K. Gilson, *Journal of Computational Chemistry* **23**, 1244 (2002).
- ¹³T. Simonson, *Reports on Progress in Physics* **66**, 737 (2003).
- ¹⁴N. A. Baker, D. Bashford, and D. A. Case, *Implicit Solvent Electrostatics in Biomolecular Simulation*, in New Algorithms for Macromolecular Simulation, edited by B. Leimkuhler et al., *Lecture Notes in Computational Science and Engineering*, pages 263–295, Springer, Berlin, Heidelberg, 2006.
- ¹⁵J. P. Bardhan, *Comput. Sci. Discov.* **5**, 013001 (2012).
- ¹⁶L. Li, C. Li, Z. Zhang, and E. Alexov, *J. Chem. Theory Comput.* **9**, 2126 (2013).
- ¹⁷W. Rocchia, E. Alexov, and B. Honig, *J. Phys. Chem. B* **105**, 6507 (2001).
- ¹⁸A. Nicholls and B. Honig, *Journal of Computational Chemistry* **12**, 435 (1991).
- ¹⁹N. A. Baker, D. Sept, S. Joseph, M. J. Holst, and J. A. McCammon, *Proc Natl Acad Sci U S A* **98**, 10037 (2001).
- ²⁰D. Chen, Z. Chen, C. Chen, W. Geng, and G.-W. Wei, *Journal of Computational Chemistry* **32**, 756 (2011).

- ²¹D. D. Nguyen, B. Wang, and G.-W. Wei, *Journal of Computational Chemistry* **38**, 941 (2017).
- ²²J. D. Jackson and R. F. Fox, *American Journal of Physics* **67**, 841 (1999).
- ²³S. Miertuš, E. Scrocco, and J. Tomasi, *Chemical Physics* **55**, 117 (1981).
- ²⁴S. Miertus and J. Tomasi, *Chemical Physics* **65**, 239 (1982).
- ²⁵L. Onsager, *Journal of the American Chemical Society* **58**, 1486 (1936).
- ²⁶J. Barker and R. Watts, *Molecular Physics* **26**, 789 (1973).
- ²⁷J. Tomasi, B. Mennucci, and R. Cammi, *Chemical Reviews* **105**, 2999 (2005).
- ²⁸D. M. Chipman, *J. Chem. Phys.* **106**, 10194 (1997).
- ²⁹D. M. Chipman, *Theor Chem Acc* **107**, 80 (2002).
- ³⁰E. Cancès, B. Mennucci, and J. Tomasi, *J. Chem. Phys.* **107**, 3032 (1997).
- ³¹V. M. Rosas-García and R. D. Gandour, *J. Am. Chem. Soc.* **119**, 7587 (1997).
- ³²M. M. Scherer, B. A. Balko, D. A. Gallagher, and P. G. Tratnyek, *Environ. Sci. Technol.* **32**, 3026 (1998).
- ³³G. Schüürmann, *J. Chem. Phys.* **109**, 9523 (1998).
- ³⁴E. V. Stefanovich, A. I. Boldyrev, T. N. Truong, and J. Simons, *J. Phys. Chem. B* **102**, 4205 (1998).
- ³⁵J.-M. Pons, M. Oblin, A. Pommier, M. Rajzmann, and D. Liotard, *J. Am. Chem. Soc.* **119**, 3333 (1997).
- ³⁶T. N. Truong and E. V. Stefanovich, *Chemical Physics Letters* **240**, 253 (1995).
- ³⁷E. V. Stefanovich and T. N. Truong, *J. Chem. Phys.* **106**, 7700 (1997).
- ³⁸A. Pomogaeva and D. M. Chipman, *J. Phys. Chem. A* **119**, 5173 (2015).
- ³⁹M. J. Huron and P. Claverie, *The Journal of Physical Chemistry* **78**, 1853 (1974).
- ⁴⁰W. H. Orttung, *J. Am. Chem. Soc.* **100**, 4369 (1978).
- ⁴¹J. Warwicker and H. Watson, *Journal of Molecular Biology* **157**, 671 (1982).
- ⁴²A. Klamt, *WIREs Computational Molecular Science* **1**, 699 (2011).
- ⁴³I. S. Tolokh et al., *Nucleic Acids Research* **42**, 10823 (2014).
- ⁴⁴B. Mennucci, M. Cossi, and J. Tomasi, *J. Chem. Phys.* **102**, 6837 (1995).
- ⁴⁵A. W. Lange and J. M. Herbert, *Chemical Physics Letters* **509**, 77 (2011).
- ⁴⁶J. Tomasi and M. Persico, *Chem. Rev.* **94**, 2027 (1994).
- ⁴⁷R. Cammi and J. Tomasi, *Journal of Computational Chemistry* **16**, 1449 (1995).
- ⁴⁸A. Klamt, *The Journal of Physical Chemistry* **99**, 2224 (1995).

- ⁴⁹M. Cossi and V. Barone, *J. Chem. Phys.* **109**, 6246 (1998).
- ⁵⁰A. Klamt, C. Moya, and J. Palomar, *J. Chem. Theory Comput.* **11**, 4220 (2015).
- ⁵¹A. Klamt and G. Schüürmann, *J. Chem. Soc., Perkin Trans. 2* **1**, 799 (1993).
- ⁵²J. C. Gordon, A. T. Fenley, and A. Onufriev, *The Journal of Chemical Physics* **129**, 075102 (2008).
- ⁵³G. Hoijtink, E. De Boer, P. Van der Meij, and W. Weijland, *Recl. Trav. Chim. Pays-Bas* **75**, 487 (1956).
- ⁵⁴S. C. Tucker and D. G. Truhlar, *Chem. Phys. Lett.* **157**, 164 (1989).
- ⁵⁵D. Qiu, P. Shenkin, F. Hollinger, and W. C. Still, *J. Phys. Chem. A* **101**, 3005 (1997).
- ⁵⁶B. Jayaram, Y. Liu, and D. J. Beveridge, *J. Chem. Phys.* **109**, 1465 (1998).
- ⁵⁷W. C. Still, A. Tempczyk, R. C. Hawley, and T. Hendrickson, *J. Am. Chem. Soc.* **112**, 6127 (1990).
- ⁵⁸A. Onufriev, D. Bashford, and D. Case, *J. Phys. Chem. B* **104**, 3712 (2000).
- ⁵⁹B. N. Dominy and C. L. Brooks, *J. Phys. Chem. B* **103**, 3765 (1999).
- ⁶⁰D. Bashford and D. Case, *Annu. Rev. Phys. Chem.* **51**, 129 (2000).
- ⁶¹N. Calimet, M. Schaefer, and T. Simonson, *Proteins: Structure, Function, and Genetics* **45**, 144 (2001).
- ⁶²G. D. Hawkins, C. J. Cramer, and D. G. Truhlar, *Chem. Phys. Lett* **246**, 122 (1995).
- ⁶³G. D. Hawkins, C. J. Cramer, and D. G. Truhlar, *J. Phys. Chem.* **100**, 19824 (1996).
- ⁶⁴M. Schaefer and M. Karplus, *J. Phys. Chem.* **100**, 1578 (1996).
- ⁶⁵M. Feig, W. Im, and C. L. Brooks, *J. Chem. Phys.* **120**, 903 (2004).
- ⁶⁶M. S. Lee, J. F. R. Salsbury, and C. L. Brooks, III, *J. Chem. Phys.* **116**, 10606 (2002).
- ⁶⁷M. S. Lee, M. Feig, F. R. Salsbury, and C. L. Brooks, *Journal of Computational Chemistry* **24**, 1348 (2003).
- ⁶⁸A. Onufriev, D. Bashford, and D. A. Case, *Proteins* **55**, 383 (2004).
- ⁶⁹T. Wang and R. Wade, *Proteins* **50**, 158 (2003).
- ⁷⁰E. Gallicchio and R. M. Levy, *J. Comp. Chem.* **25**, 479 (2004).
- ⁷¹H. Nymeyer and A. E. García, *Proc Natl Acad Sci U S A* **100**, 13934 (2003).
- ⁷²A. Ghosh, C. S. Rapp, and R. A. Friesner, *J. Phys. Chem. B* **102**, 10983 (1998).
- ⁷³M. Scarsi, J. Apostolakis, and A. Caffisch, *J. Phys. Chem. A* **101**, 8098 (1997).
- ⁷⁴W. Im, M. S. Lee, and C. L. Brooks, *Journal of Computational Chemistry* **24**, 1691 (2003).

- ⁷⁵U. Haberthür and A. Caffisch, *J Comput Chem* **29**, 701 (2007).
- ⁷⁶J. A. Grant, B. T. Pickup, M. J. Sykes, C. A. Kitchen, and A. Nicholls, *Phys. Chem. Chem. Phys.* **9**, 4913 (2007).
- ⁷⁷H. Tjong and H. X. Zhou, *J. Phys. Chem. B* **111**, 3055 (2007).
- ⁷⁸P. Labute, *Journal of Computational Chemistry* **29**, 1693 (2008).
- ⁷⁹A. Onufriev, D. A. Case, and D. Bashford, *Journal of Computational Chemistry* **23**, 1297 (2002).
- ⁸⁰A. V. Onufriev and G. Sigalov, *The Journal of Chemical Physics* **134**, 164104+ (2011), PMID: PMC3100913.
- ⁸¹A. W. Lange and J. M. Herbert, *J. Chem. Theory Comput.* **8**, 1999 (2012).
- ⁸²C. Simmerling, B. Strockbine, and A. E. Roitberg, *J. Am. Chem. Soc.* **124**, 11258 (2002).
- ⁸³J. Chen, W. Im, and C. L. Brooks, *J Am Chem Soc* **128**, 3728 (2006).
- ⁸⁴H. Lei and Y. Duan, *J. Phys. Chem. B* **111**, 5458 (2007).
- ⁸⁵J. W. Pitera and W. Swope, *Proc Natl Acad Sci U S A* **100**, 7587 (2003).
- ⁸⁶A. Jagielska and H. A. Scheraga, *Journal of Computational Chemistry* **28**, 1068 (2007).
- ⁸⁷V. Hornak, A. Okur, R. C. Rizzo, and C. Simmerling, *Proc Natl Acad Sci U S A* **103**, 915 (2006).
- ⁸⁸R. E. Amaro, X. Cheng, I. Ivanov, D. Xu, and A. J. Mccammon, *Journal of the American Chemical Society* **131**, 4702 (2009).
- ⁸⁹J. Z. Ruscio and A. Onufriev, *Biophys. J.* **91**, 4121 (2006), PMID 1635688.
- ⁹⁰J. Chocholousová and M. Feig, *J. Phys. Chem. B* **110**, 17240 (2006).
- ⁹¹W. Zheng, V. Spassov, L. Yan, P. Flook, and S. Szalma, *Computational Biology and Chemistry* **28**, 265 (2004).
- ⁹²J. Zhu, E. Alexov, and B. Honig, *The journal of physical chemistry. B* **109**, 3008 (2005).
- ⁹³A. V. Onufriev and D. A. Case, *Annual Review of Biophysics* **48**, 275 (2019).
- ⁹⁴D. L. Mobley and J. P. Guthrie, *Journal of Computer-Aided Molecular Design* **28**, 711 (2014).
- ⁹⁵D. L. Mobley, C. I. Bayly, M. D. Cooper, M. R. Shirts, and K. A. Dill, *Journal of Chemical Theory and Computation* **11**, 1347 (2015).
- ⁹⁶A. Mukhopadhyay, B. H. Aguilar, I. S. Tolokh, and A. V. Onufriev, *Journal of Chemical Theory and Computation* **10**, 1788 (2014).
- ⁹⁷D. A. Case et al., *Journal of Computational Chemistry* **26**, 1668 (2005).

- ⁹⁸M. Ramanadham, L. C. Sieker, and L. H. Jensen, *Acta Crystallographica Section B Structural Science* **46**, 63 (1990).
- ⁹⁹X. Wang, J. Lan, J. Ge, J. Yu, and S. Shan, Crystal structure of SARS-CoV-2 spike receptor-binding domain bound with ACE2, <https://www.rcsb.org/structure/6M0J>, 2020.
- ¹⁰⁰J. C. Gordon et al., *Nucleic Acids Res* **33**, W368 (2005).
- ¹⁰¹F. M. Richards, *Annual Review of Biophysics and Bioengineering* **6**, 151 (1977).
- ¹⁰²A. Bondi, *The Journal of Physical Chemistry* **68**, 441 (1964).
- ¹⁰³S. Decherchi and W. Rocchia, *PLoS ONE* **8**, e59744 (2013).
- ¹⁰⁴J. G. Kirkwood, *The Journal of Chemical Physics* **2**, 351 (1934).
- ¹⁰⁵A. T. Fenley, J. C. Gordon, and A. Onufriev, *The Journal of Chemical Physics* **129**, 075101 (2008).
- ¹⁰⁶D. Bashford, An object-oriented programming suite for electrostatic effects in biological molecules An experience report on the MEAD project, in *Scientific Computing in Object-Oriented Parallel Environments*, edited by Y. Ishikawa, R. R. Oldehoeft, J. V. W. Reynders, and M. Tholburn, *Lecture Notes in Computer Science*, pages 233–240, Berlin, Heidelberg, 1997, Springer.
- ¹⁰⁷B. Honig, K. Sharp, and A. S. Yang, *The Journal of Physical Chemistry* **97**, 1101 (1993).
- ¹⁰⁸G. Sigalov, A. Fenley, and A. Onufriev, *The Journal of Chemical Physics* **124**, 124902 (2006).
- ¹⁰⁹A. Onufriev, D. Bashford, and D. A. Case, *Proteins: Structure, Function, and Bioinformatics* **55**, 383 (2004).
- ¹¹⁰G. Sigalov, P. Scheffel, and A. Onufriev, *The Journal of Chemical Physics* **122**, 094511 (2005).
- ¹¹¹E. L. Coitiño, J. Tomasi, and R. Cammi, *Journal of Computational Chemistry* **16**, 20 (1995).
- ¹¹²J. A. Grant, R. L. Williams, and H. A. Scheraga, *Biopolymers* **30**, 929 (1990).
- ¹¹³C. S. Pomelli, J. Tomasi, and V. Barone, *Theoretical Chemistry Accounts: Theory, Computation, and Modeling (Theoretica Chimica Acta)* **105**, 446 (2001).
- ¹¹⁴R. Cammi et al., *The Journal of Chemical Physics* **117**, 13 (2002).
- ¹¹⁵E. V. Katkova, A. V. Onufriev, B. Aguilar, and V. B. Sulimov, *Journal of Molecular Graphics and Modelling* **72**, 70 (2017).

- ¹¹⁶S. Izadi, R. C. Harris, M. O. Fenley, and A. V. Onufriev, *J. Chem. Theory Comput.* **14**, 1656 (2018).
- ¹¹⁷C. C. F. Blake et al., *Proceedings of the Royal Society of London. Series B. Biological Sciences* **167**, 378 (1967).
- ¹¹⁸A. Warshel and M. Levitt, *Journal of Molecular Biology* **103**, 227 (1976).
- ¹¹⁹Z. Li and T. Lazaridis, *Physical Chemistry Chemical Physics* **9**, 573 (2007).
- ¹²⁰S. B. de Beer, N. P. Vermeulen, and C. Oostenbrink, *Current Topics in Medicinal Chemistry* **10**, 55 (2010).
- ¹²¹F. Spyraakis et al., *J. Med. Chem.* **60**, 6781 (2017).
- ¹²²D. Hamelberg and J. A. McCammon, *J. Am. Chem. Soc.* **126**, 7683 (2004).
- ¹²³M. Petřek et al., *BMC Bioinformatics* **7**, 316 (2006).
- ¹²⁴I. S. Tolokh et al., *Nucleic acids research* **42**, 10823 (2014), PMID: PMC25123663.
- ¹²⁵J. Zahradník et al., *bioRxiv* , 2021.01.06.425392 (2021).